



Multipoint Observations of Magnetic Reconnection in the Martian Magnetotail Triggered by an Interplanetary Magnetic Field Rotation

Yuanzheng Wen¹, Jasper S. Halekas¹, Han-Wen Shen¹, Abigail R. Azari^{2,3,4}, David A. Brain⁵, Yaxue Dong⁵, David L. Mitchell⁶, Christian X. Mazelle⁷, Jared R. Espley⁸, and James P. McFadden⁶

¹ Department of Physics and Astronomy, University of Iowa, Iowa City, IA, USA; yuanzheng-wen@uiowa.edu

² Department of Physics, University of Alberta, Edmond, AB, Canada

³ Department of Electrical and Computer Engineering, University of Alberta, Edmond, AB, Canada

⁴ Alberta Machine Intelligence Institute, Edmonton, AB, Canada

⁵ Laboratory for Atmospheric and Space Physics, University of Colorado, Boulder, CO, USA

⁶ Space Sciences Laboratory, University of California at Berkeley, Berkeley, CA, USA

⁷ Institut de Recherche en Astrophysique et Planétologie (IRAP), Toulouse, France

⁸ Solar System Exploration Division, NASA Goddard Space Flight Center, Greenbelt, MD, USA

Received 2025 January 27; revised 2025 March 5; accepted 2025 March 5; published 2025 March 26

Abstract

The induced magnetosphere of Mars is highly dynamic, driven by both the upstream solar wind and the planet's crustal magnetic fields. This variability can occur on timescales much shorter than a single spacecraft orbit, making it difficult to distinguish between spatial and temporal variations in the induced magnetosphere. In this study, we utilize simultaneous multipoint observations from the Mars Atmosphere and Volatile Evolution (MAVEN) and Tianwen-1 missions to investigate how the induced magnetosphere responds to dynamic changes in the solar wind. We report a magnetic reconnection event observed by MAVEN in the Martian magnetotail, occurring a few minutes after an interplanetary magnetic field (IMF) rotation observed by Tianwen-1 in the upstream solar wind. This reconnection event is characterized by clear Hall magnetic field signatures and high-speed ion jets, indicating the presence of a diffusion region. Our analysis of the change in the magnetic field morphology suggests that this reconnection was likely triggered by this IMF rotation, occurring during the resulting reconfiguration of the induced magnetosphere. This multipoint study demonstrates the important role of dynamic upstream solar wind conditions, particularly IMF rotations, in driving the plasma processes in the Martian magnetotail, contributing to our understanding of solar wind energy and momentum transfer and their roles in ion escape in Mars's hybrid magnetosphere.

Unified Astronomy Thesaurus concepts: Mars (1007); Solar wind (1534); Planetary magnetospheres (997); Space plasmas (1544); Solar-planetary interactions (1472); Planetary science (1255); Star-planet interactions (2177)

1. Introduction

Mars lacks a strong intrinsic magnetic field, making its interaction with the solar wind and the interplanetary magnetic field (IMF) fundamentally different from that of Earth. The solar wind interacts directly with the Martian ionosphere and upper atmosphere (A. Nagy et al. 2004; C. Bertucci et al. 2011; J. S. Halekas et al. 2021). This direct interaction induces ionospheric currents, leading to the draping and piling up of the IMF around the planet, which forms an induced magnetosphere. Mass loading from ionized atmospheric heavy ions slows and deflects the solar wind flow, further shaping the structure of the Martian induced magnetosphere. Additionally, Mars has localized crustal magnetic fields (M. Acuna et al. 1999), particularly concentrated in the southern hemisphere, which adds further complexity to its magnetospheric structure and plasma dynamics (Y. Ma et al. 2002; D. Brain et al. 2003; E. Dubinin et al. 2023). The interaction between the solar wind, the induced magnetosphere, and the localized crustal fields creates a highly variable and dynamic plasma environment, where various plasma processes such as magnetic reconnection can occur. Magnetic reconnection is a fundamental process in

space plasma physics, which can cause a rapid change in magnetic field topology and simultaneously convert magnetic energy into kinetic particle energy (D. J. Gershman et al. 2024; H. Hasegawa et al. 2024). It plays a crucial role in controlling the transfer of energy and mass in plasma environments throughout the solar system. Reconnection has been widely observed on both magnetized (A. Masters et al. 2012; J. Burch et al. 2016; R. W. Ebert et al. 2017; D. J. Gershman et al. 2024; J. Joseph et al. 2024) and unmagnetized planets (J. Eastwood et al. 2008; T. Zhang et al. 2012), as well as at comets (M. B. Niedner 1984; C. Russell et al. 1986) and in the solar wind (J. Gosling 2012).

At Mars, magnetic reconnection can take place in multiple plasma regions, including the magnetotail (J. Eastwood et al. 2008; J. Halekas et al. 2009; Y. Harada et al. 2015, 2017), the boundary of the induced magnetosphere (J. Wang et al. 2021; R. Lin et al. 2024), the magnetosheath (X. Xu et al. 2023), and even within the ionosphere (T. Cravens et al. 2020). The crustal magnetic fields further complicate these processes, as magnetic reconnection can also occur between the IMF and the crustal fields, both on the dayside and nightside (Y. Harada et al. 2018; R. Lin et al. 2024; Y. Ye et al. 2024). Furthermore, reconnection can also take place between different regions of the crustal fields themselves (G. Chen et al. 2023; R. Lin et al. 2023), adding to the complexity of the Martian plasma environment. Magnetic reconnection contributes to heating and accelerating particles in the Martian magnetosphere and



Original content from this work may be used under the terms of the [Creative Commons Attribution 4.0 licence](https://creativecommons.org/licenses/by/4.0/). Any further distribution of this work must maintain attribution to the author(s) and the title of the work, journal citation and DOI.

can lead to substantial ion loss, a factor in atmospheric erosion (D. Brain et al. 2010; C. Zhang et al. 2021; L. Wang et al. 2022, 2023; Y. Ye et al. 2024). One of the key factors influencing magnetic reconnection at Mars is the upstream solar wind conditions, including changes in the IMF. Variations in the IMF, particularly sudden rotations or polarity changes, may lead to the formation of antiparallel magnetic fields in the Martian induced magnetosphere, creating favorable conditions for reconnection (J. Halekas et al. 2009; Y. Harada et al. 2015).

Analogous processes have been studied at Venus, another planet with an induced magnetosphere but without crustal magnetic fields. N. J. Edberg et al. (2011) investigated atmospheric erosion at Venus during active space weather conditions caused by corotating interaction regions (CIRs) and interplanetary coronal mass ejections (ICMEs). They observed that atmospheric escape rates increased significantly during these events and suggested that changes in the IMF polarity during CIRs/ICMEs could trigger magnetic reconnection in the Venusian induced magnetosphere. D. Vech et al. (2016) also conducted a statistical study on the effects of heliospheric current sheet crossings on the Venusian induced magnetosphere. They found that the polarity reversal of the IMF leads to a reconfiguration of the induced magnetosphere with opposite polarity. Their results show a significant enhancement in the heavy ion flux in the Venusian magnetotail after IMF polarity reversal events. This suggests that magnetic reconnection might be occurring on both the dayside and nightside, disconnecting the plasma tail from the planetary ionosphere. They further suggested that this process may take place on very short timescales, possibly within a few minutes. While these studies at Venus provide valuable insights, the observations were limited by the use of a single spacecraft, which cannot fully capture the temporal and spatial evolution of magnetic reconnection processes triggered by IMF rotations. The inability to simultaneously observe upstream solar wind conditions and downstream magnetotail responses makes it challenging to definitively link IMF rotations to magnetic reconnection events.

In this study, we addressed this limitation by utilizing observations from two spacecraft, the Mars Atmosphere and Volatile Evolution (MAVEN) mission (B. M. Jakosky et al. 2015) and the Tianwen-1 orbiter (W. Wan et al. 2020; Y. Zou et al. 2021). This dual-spacecraft approach allows us to simultaneously monitor both the upstream solar wind conditions (especially the IMF) and the induced magnetosphere of Mars (Z. Guo et al. 2024). This Letter presents the joint observation by MAVEN and Tianwen-1 of a magnetic reconnection event in the Martian magnetotail, likely triggered by an IMF rotation, providing insights into the dynamic evolution of the Martian induced magnetospheric structure.

2. Data and Observations

The data used in this study are from the MAVEN and Tianwen-1 missions. Magnetic field measurements were made by both MAVEN and Tianwen-1. The Magnetometer (MAG) instrument (J. Connerney et al. 2015) onboard the MAVEN spacecraft provides three-dimensional magnetic field vector measurements with a cadence of up to 32 samples per second. Similarly, Tianwen-1's Mars Orbiter Magnetometer (MOMAG) instrument (K. Liu et al. 2020; Y. Wang et al. 2023; Z. Zou et al. 2023; G. Wang et al. 2024) records

magnetic field vectors at a sampling rate of 32 samples per second. The MAG and MOMAG data binned at a 1 s time resolution are used in this study. The Solar Wind Ion Analyzer provides three-dimensional distributions of ions in the energy range of 25 eV–25 keV and their moments data derived from this distribution at a time resolution of 4 s (J. Halekas et al. 2015, 2017). The MAVEN Solar Wind Electron Analyzer (SWEA) instrument provides electron energy spectrograms and pitch angle distribution at a temporal resolution of 2 s (D. Mitchell et al. 2016). The Suprathermal and Thermal Ion Composition (STATIC) instrument is equipped with an electrostatic top-hat analyzer and a time-of-flight velocity analyzer, allowing it to detect ions with energies ranging from 0.1 eV to 30 keV within a field of view of $360^\circ \times 90^\circ$. Its unique capabilities enable the identification of ion species according to their masses, with a cadence of 4 s (J. McFadden et al. 2015). Detailed ion (H^+ , O^+ , O_2^+) moments, including density and velocity, can be calculated from the corresponding three-dimensional particle distributions.

Figure 1 provides an overview of an event that was jointly observed by MAVEN and Tianwen-1 between 01:10:00 and 01:25:00 UT on 2021 December 5. During this period, MAVEN was moving in the Martian magnetotail, while Tianwen-1 was positioned in the upstream solar wind, as shown in Figure 1(a) (trajectories of the two spacecraft in the $X_{MISO}-Z_{MISO}$ and $X_{MISO}-Y_{MISO}$ planes are shown in Figure A1 in Appendix). Both the magnetic field and plasma data are presented in the Mars Solar Orbital (MSO) coordinate system, where the X -axis points from the center of Mars to the Sun, the Z -axis points to the north pole of Mars's orbital plane, and the Y -axis completes the right-handed orthogonal coordinate system.

As shown in Figure 1(b), Tianwen-1 observed a rapid IMF rotation in the upstream solar wind, with both the B_x and B_z components shifting from positive to negative values. About 2 minutes later, MAVEN encountered a current sheet in the magnetotail, marked by a significant decrease in magnetic field strength and a reversal of the B_x component from negative to positive (Figure 1(c)). This event was accompanied by an increase in ion and electron energy fluxes as shown in Figures 1(g)–(j). Within the core of the current sheet, there is a notable enhancement in the ion velocity, especially for protons (Figures 1(d)–(f)). It is important to note that the velocity vectors for O^+ and O_2^+ ions between 01:12 and 01:16 UT are unreliable (shaded region), as the ion fluxes observed by MAVEN during this interval were too low. The observed enhancement in tailward ion flow can be interpreted as ion outflow, and the occurrence of ion outflow and the reversal of the B_x component suggests that magnetic reconnection may have occurred within this current sheet (Y. Harada et al. 2015, 2017; R. Lin et al. 2024).

A detailed analysis of the current sheet's characteristics is necessary to provide comprehensive evidence for the occurrence of magnetic reconnection. We transformed both the magnetic field and ion velocity vectors from the MSO coordinate system into the local LMN coordinate system (L is along the antiparallel magnetic field direction, M is along the X line, and N is along the current sheet normal) for the period between 01:17:00 and 01:22:00 UT. The LMN coordinates over this interval were determined using the minimum variance analysis (MVA) method (B. U. Sonnerup 1998), which is a technique for defining the local current sheet geometry. The eigenvectors

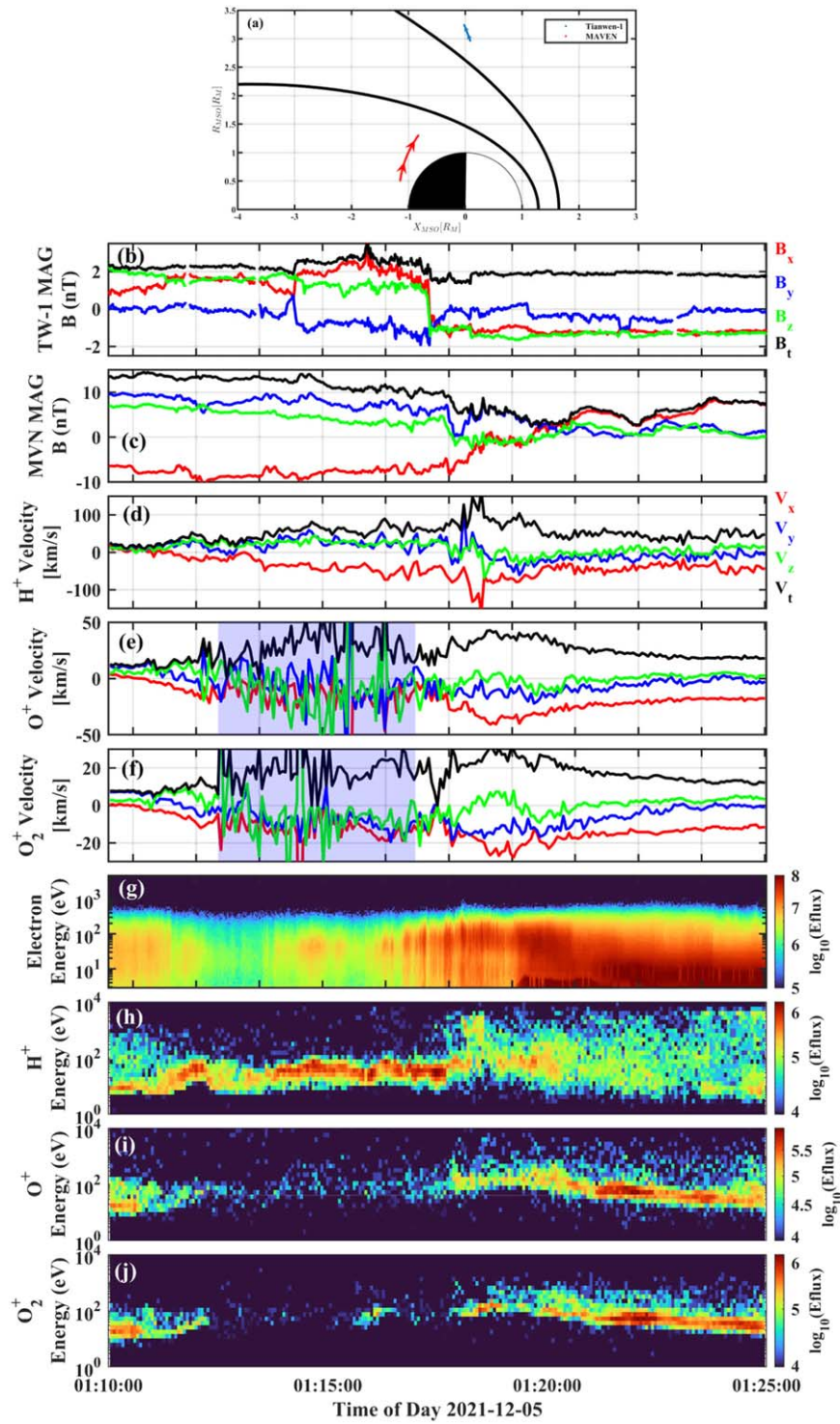


Figure 1. Overview of the current sheet crossing event on 2021 December 5 during 01:10:00–01:25:00 UT. (a) Orbits of MAVEN and Tianwen-1 in the X–R plane, $R = \sqrt{Y^2 + Z^2}$. The black curve represents the bow shock and induced magnetosphere boundary models based on D. Vignes et al. (2000). (b) Tianwen-1 magnetic field data in MSO coordinates. (c) MAVEN magnetic field data in MSO coordinates. ((d), (e), (f)) Velocity components of O^+ , H^+ , and O_2^+ , respectively, in MSO coordinates. (g) Electron spectrogram from MAVEN SWEA. ((h), (i), (j)) O^+ , H^+ , and O_2^+ energy spectrograms from MAVEN STATIC.

calculated from the MVA correspond to the following orientations in MSO coordinates: $L = [0.94, -0.35, 0.025]$, $M = [0.11, 0.23, -0.97]$, and $N = [0.33, 0.91, 0.26]$. The reliability of the LMN transformation is confirmed by the eigenvalue ratios ($\lambda_1/\lambda_2 = 6.73$ and $\lambda_2/\lambda_3 = 6.93$), ensuring accurate alignment for analyzing the reconnection region.

As shown in Figure 2(a), the magnetic field B_L component reversed polarity from negative to positive, while the B_M component exhibited a bipolar structure, transitioning from positive to negative. Meanwhile, the B_N component remained positive and relatively stable throughout the event. These magnetic signatures are characteristics of Hall magnetic fields,

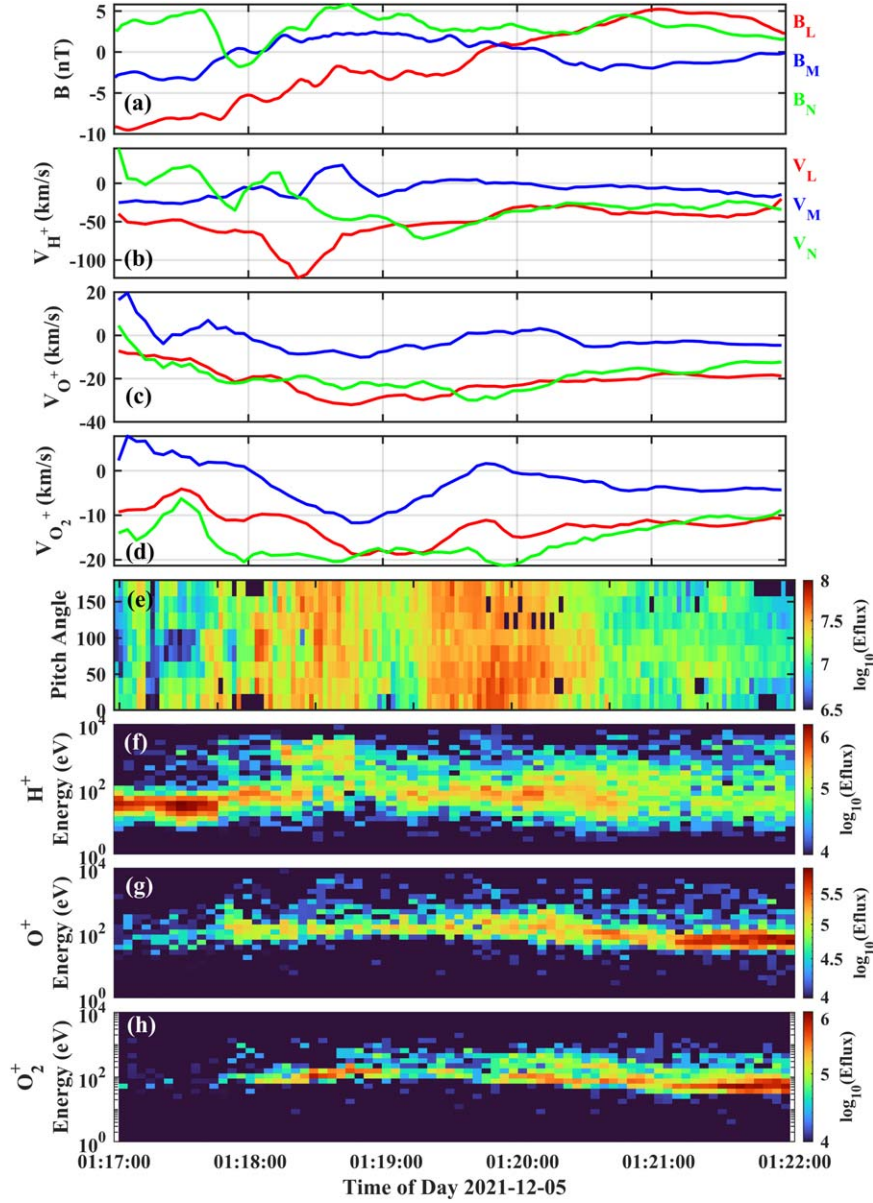


Figure 2. Zoom-in view of the event during 01:17:00–01:22:00 UT on 2021 December 5. (a) Three components of the magnetic field in LMN coordinates. (b)–(d) Velocity components of H^+ , O^+ , and O_2^+ ions in LMN coordinates. (e) Pitch angle distribution of electrons in the energy range of 111–140 eV. (f)–(h) Energy spectrograms of H^+ , O^+ , and O_2^+ , respectively.

which are indicators of the ion diffusion region during the collisionless magnetic reconnection (J. Eastwood et al. 2008; J. Halekas et al. 2009; Y. Harada et al. 2017). The $B_L - B_M$ pattern is consistent with a crossing tailward of the X line, specifically of type 4 polarity, as shown in Figure 1 of Y. Harada et al. (2017). This indicates that the ion diffusion region possibly associated with a magnetic reconnection event was observed.

In conjunction with the magnetic field data, ion velocity measurements in Figures 2(b)–(d) revealed a pronounced tailward flow in the V_L component, with H^+ ions reaching negative velocities up to 100 km s^{-1} during the current sheet crossing (Figure 2(b)). Interestingly, this tailward velocity enhancement is less pronounced for O^+ and O_2^+ ions, which show only slight negative V_L enhancements. Additionally, as shown in Figures 2(f)–(h), within the ion diffusion region (approximately between 01:18:30 and 01:20:10 UT), we

observed that protons were significantly energized, with their energy increasing by nearly 2 orders of magnitude. However, for the heavier ions (O^+ and O_2^+), the energy spectrograms show only slight enhancements. These features of H^+ and heavier ions are also consistent with the expected ion jet direction in the reconnection outflow for a type 4 tailward X line crossing (Y. Harada et al. 2017). The distinct behaviors of different ion species are expected, with protons experiencing greater acceleration than heavier ions due to their lower mass and stronger coupling to the magnetic field. In contrast, O^+ and O_2^+ ions, because of their larger masses, remain less affected and stay largely unmagnetized within the ion diffusion region (Y. Liu et al. 2015; Y. Harada et al. 2017).

Meanwhile, the pitch angle distribution of electrons shown in Figure 2(e) exhibited one-sided loss cones (around 01:19:00 UT) before the reconnection region crossing, indicating the presence of an open magnetic field topology (D. Brain

et al. 2007; T. Weber et al. 2017; S. Xu et al. 2019). On the other side of the reconnection region, after the crossing, however, we observed more isotropic electron distributions, with no clear loss cone features. This isotropy may be attributed to electron scattering caused by various mechanisms like wave-particle interaction and magnetic field line curvature in the vicinity of the reconnection region (Y. Zhang et al. 2016; Z. Guo et al. 2022; T. Li et al. 2023; J. Wang et al. 2023). Enhanced wave activity was indeed detected by MAVEN during this interval (not shown here), which further supports this interpretation.

To further confirm the magnetic reconnection qualitatively, we conducted a Walén test analysis (T. Phan et al. 2004; Y. Zhang 2016; G. Poh et al. 2021) during this interval. The outflow generated by magnetic reconnection is expected to accelerate to the local Alfvén speed $V_A = \frac{B}{\sqrt{\mu_0 \rho}}$, where B represents the magnetic field and ρ is the total plasma mass density (H^+ , O^+ , O_2^+). By comparing the observed average flow velocity $V' = V - V_{HT}$ in the de Hoffmann-Teller frame (F. De Hoffmann & E. Teller 1950) with the local Alfvén velocity, we can assess whether the flow may be a result of magnetic reconnection.

The results of the Walén test for our case study are presented as a correlation between the observed flow velocity V' and the calculated Alfvén speed V_A (see Figure B1 in Appendix). The Walén test shows a slope of 0.39 with a high correlation coefficient (CC) of 0.82 before the current sheet crossing, indicating partially Alfvénic but sub-Alfvénic plasma flows. After the crossing, the slope became -1.07 , closer to an ideal Alfvénic response, while the CC decreased to 0.59, suggesting increased variability. These observations align with the expected signatures of magnetic reconnection, where the transition from sub-Alfvénic to Alfvénic ion flow accompanied by changes in plasma flow direction further supports our interpretation.

3. Discussion and Conclusions

In this study, we have provided a detailed analysis of a possible magnetic reconnection event observed by MAVEN in the Martian magnetotail. It is important to note that magnetic reconnection events have been extensively observed by MAVEN across various plasma regions of Mars, as discussed in Section 1. Due to the complex structure of Mars's induced magnetosphere, reconnection can be triggered at different locations, including between draped antiparallel IMF lines at the center of the magnetotail, and between the IMF and the crustal magnetic fields (J. Halekas et al. 2009). A key question for this event is whether the observed reconnection was triggered by the upstream IMF rotation or other mechanisms.

To further investigate this hypothesis, we first calculated the crustal magnetic fields with the model by J. Gao et al. (2021) during this observational period to assess their influence on the magnetic field measurements by MAVEN. Our analysis revealed that the local contribution of the crustal magnetic field during this interval is negligible given its magnitude is near zero. In addition, MAVEN's location is in the northern hemisphere and also far away from strong crustal magnetic fields in geographical coordinates, further suggesting that the reconnection was unlikely triggered by crustal magnetic fields, though distant crustal magnetic fields could still be able to affect the global structure of the magnetotail (G. A. DiBraccio

et al. 2018, 2022; J. Zhou et al. 2024). Furthermore, it is also necessary to assess whether this event represents a typical magnetic reconnection between the oppositely draped IMF lines across the magnetotail current sheet. One potential method for verifying this is to show the draped magnetic field morphology before and after the IMF rotation, subsequently comparing the MAVEN observations with the expected morphology. There are existing statistical models of the magnetic field morphology under different IMFs (C. Zhang et al. 2022) and IMFs combined with crustal field conditions (e.g., A. Azari et al. 2023). These statistics-based models take advantage of multiple temporal observations and are thus limited to before and after comparisons for a single temporal event. A more sophisticated, time-dependent physical model may be required to further compare, which is beyond the scope and capacity of this study.

The availability of multipoint observations from both MAVEN and Tianwen-1 provides a solution for comparison to statistical models. With Tianwen-1 positioned in the upstream solar wind, we can obtain critical measurements of the upstream magnetic field and solar wind velocity. By incorporating these measurements, we can further transform the MAVEN spacecraft coordinates and the magnetic field data from MSO coordinates into Mars Solar Electric (MSE) coordinates (X_{MSE} points antiparallel to the upstream solar wind flow, Y_{MSE} points along the crossflow magnetic field component of the upstream IMF, and Z_{MSE} points along the direction of the convection electric field in the solar wind; C. Zhang et al. 2022; H.-W. Shen et al. 2024) and project MAVEN's trajectories, along with the magnetic field vectors, onto an average magnetic field draping pattern in MSE coordinates constructed by C. Zhang et al. (2022), as shown in Figure 3. This transformation enables us to compare the observed magnetic field configurations before and after the IMF rotation with the expected draping patterns. As illustrated in Figure 3(a), MAVEN was initially traversing the $-B_x$ hemisphere before the IMF rotation, with a magnetic field direction consistent with the expected magnetic field draping pattern. If there was not an IMF rotation, we would have expected possible continuous observations of the tailward magnetic field in the $-B_x$ hemisphere. Following the IMF rotation, MAVEN's trajectory rapidly shifted to the $+B_x$ hemisphere, and the magnetic field direction flipped about 2 minutes later to the sunward direction, as indicated by the dashed black arrow. The response time delay of magnetic field clock angle change in this event is estimated to be 6 s, based on the method outlined in Z. Guo et al. (2024), while the observed timescale is approximately 15 s. It is important to note that the propagation speed in Z. Guo et al. (2024) is based on the solar wind velocity; therefore, the discrepancy in terms of time delay may be attributed to the deceleration of the solar wind as it interacts with the Martian induced magnetosphere (J. Halekas et al. 2017). This rapid transition in both MAVEN's trajectory and the magnetic field orientation aligns with the predicted magnetic field draping pattern, further supporting the expectation that the Martian induced magnetosphere reconfigured in response to the IMF rotation. Notably, MAVEN's trajectory remained outside of the central region of the magnetotail throughout the interval, indicating that this was likely not a typical current sheet crossing. Furthermore, if a current sheet flapping motion had been responsible for the observed magnetic field change, we would expect multiple crossings or

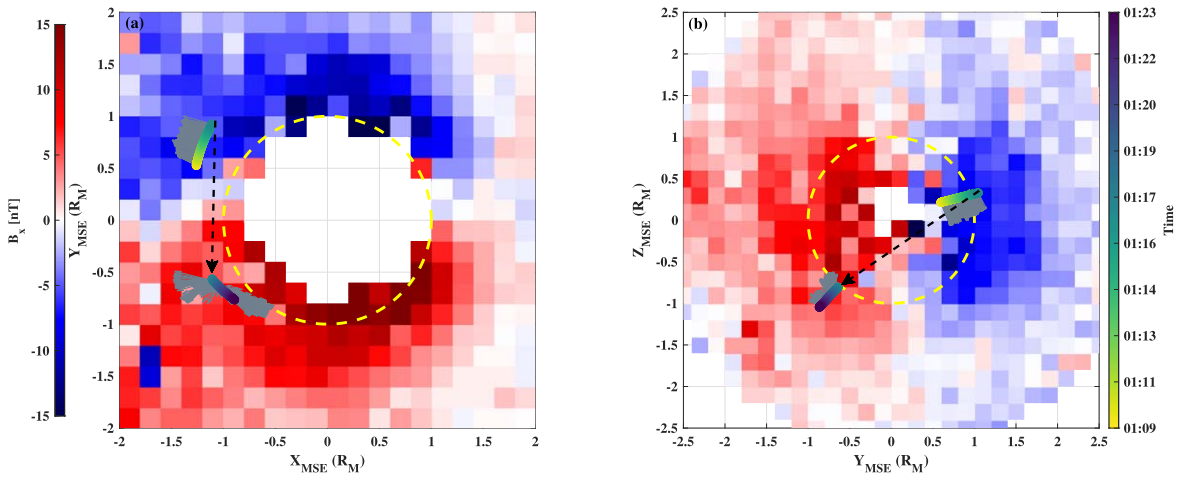


Figure 3. Average magnetic field draping map in MSE coordinates from C. Zhang et al. (2022), shown in the XY (a) and YZ (b) planes. The color map represents the B_x component, with red indicating sunward and blue indicating tailward directions. MAVEN’s trajectory in MSE coordinates is shown with colored lines, and gray arrows indicate the magnetic field direction recorded by MAVEN. The dashed black arrow indicates the rapid transition of MAVEN’s trajectory in MSE coordinates after the IMF rotation.

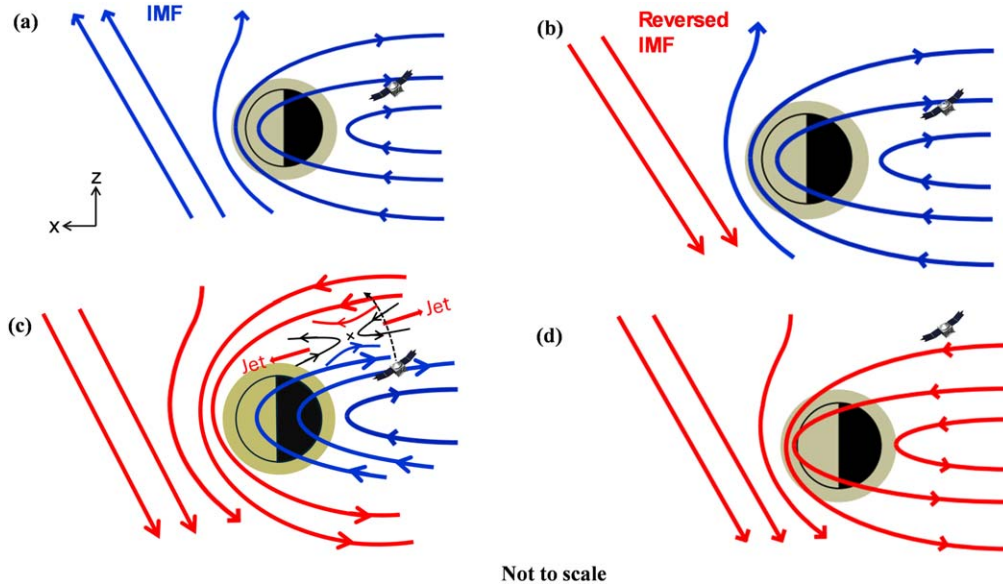


Figure 4. Schematic representation of the reconfiguration of Mars’s induced magnetosphere in response to the IMF rotation. (a) The induced magnetosphere of Mars before the IMF rotation. (b) The IMF rotates and the reversed IMF starts to drape around Mars. (c) MAVEN observed a magnetic reconnection between the oppositely directed draped magnetic field lines, leading to the formation of Hall magnetic fields and ion jets. Panel (d) illustrates the final reconfiguration after the IMF rotation, with newly draped magnetic field lines surrounding Mars. Modified based on N. J. Edberg et al. (2011).

oscillatory behavior between the lobes as the current sheet moved across MAVEN’s path (G. A. DiBraccio et al. 2017; C. Zhang et al. 2023b; Z. Guo et al. 2024). Instead, we observed a single rapid transition from the $-B_x$ to the $+B_x$ hemisphere, without strong signatures of such oscillatory dynamics. This stable lobe transition, occurring in alignment with the IMF rotation, supports the interpretation that the observed magnetic reconnection was a possible result of the IMF rotation, rather than fluctuations or shifts within the tail current sheet.

To illustrate the possible full scenario suggested by our analysis, we sketched a diagram (Figure 4) that highlights how an IMF rotation in the upstream solar wind could possibly trigger the magnetic reconnection observed by MAVEN in the magnetotail. The red and blue lines in the figure represent the IMF before and after the polarity reversal observed by Tianwen-1, respectively. Figure 4(a) shows the prerotation

configuration of the induced magnetosphere, where the IMF systematically drapes around the planetary obstacle, creating oppositely oriented magnetic fields within the magnetotail. During this phase, MAVEN was traversing the negative B_x hemisphere. As shown in Figure 4(b), the IMF undergoes a polarity reversal. The newly arriving reversed IMF, shown in blue, begins to compress against the preexisting draped magnetic field. This convergence of oppositely directed magnetic field lines creates favorable conditions for magnetic reconnection, indicated by the “X” in Figure 4(c). At this point, MAVEN observed the characteristic Hall magnetic field signature and accelerated ions associated with the magnetic reconnection process. Figure 4(d) illustrates the subsequent reconfiguration of the induced magnetosphere. However, it should be noted that, at low-altitude regions like the ionosphere, the preexisting or “fossil” induced magnetic field lines should persist for a longer duration (hours) before fully

reconfiguring. This is due to the slower plasma transport caused by mass loading effects, which delays the propagation of the new IMF to these regions, as reported in previous studies (C. Bertucci et al. 2008; D. Vech et al. 2016). Finally, the induced magnetosphere has completely changed its polarity in the magnetotail and reconfigured itself with the new IMF orientation. It should be pointed out that the magnetic reconnection may also have occurred at other regions like the dayside magnetosphere or the boundary when the IMF rotated, as suggested in previous studies (C. Bertucci et al. 2008; N. J. Edberg et al. 2011; D. Vech et al. 2016).

A significant enhancement in the density of heavy ions (O^+ and O_2^+) in the magnetotail was also observed following the magnetic reconnection event (Figure C1 in Appendix). This raises a question: is this increase directly triggered by the magnetic reconnection, or is it a result of the broader reconfiguration of Mars’s induced magnetosphere because of the IMF rotation? Previous studies (E. Dubinin et al. 2019; S. Inui et al. 2019) have revealed that the density of heavy ions is typically higher in the southern hemisphere compared to the north in MSE coordinates. Given that MAVEN’s MSE position shifted from the northern to the southern hemisphere, as shown in Figure 3(b), after the IMF rotation, this hemispheric asymmetry may explain the observed increase in the density of heavy ions. Hybrid simulations by R. Modolo et al. (2012) demonstrated that the spatial distribution of high-energy pickup ions can adjust rapidly (~ 2 minutes) to changes in the IMF orientation. Lower-energy ions inside the magnetosphere may respond differently. N. Romanelli et al. (2018, 2019) suggested that the recovery timescales of the Martian induced magnetosphere after an IMF rotation range from 8 s to 11 minutes, depending on the region, which is consistent with the observed timescale (~ 2 minutes) for the transition in the density of heavy ions.

Further modeling and multipoint observations are necessary to explore the detailed ion distribution variations in response to IMF rotations. N. Romanelli et al. (2018) also reported that H^+ and O^+ loss rates showed little correlation with changes in the IMF orientation in their hybrid simulations. More recently, MHD simulations by S. Sakai et al. (2023) showed that during IMF rotations, ion escape rates remained largely unchanged in the unmagnetized case, but increased by a factor of 50 for the magnetized case with a dipole field (100 nT) due to magnetic reconnections occurring across multiple regions of the magnetospheric flanks. While Mars lacks a global intrinsic dipole field, its strong crustal magnetic fields may act as localized “mini-magnetospheres,” and some observed features resemble those of intrinsic magnetospheres (K. Fan et al. 2023; C. Zhang et al. 2023a). This suggests that the Martian magnetosphere may represent an intermediate case, where both unmagnetized and magnetized behaviors may coexist. Consequently, how ion escape rates respond to rapid IMF

rotations on Mars remains an open question. This further emphasizes the importance of future research to examine the dependence of ion escape on IMF rotation, particularly over short timescales, using multipoint observations (B. Sánchez-Cano et al. 2022).

In summary, we have identified a possible magnetic reconnection event in the Martian magnetotail based on MAVEN observations, likely triggered by an upstream IMF rotation recorded by Tianwen-1. The observed variation in the magnetic field draping pattern around Mars indicates that this event may have resulted from magnetic reconnection between draped IMF lines with opposite directions, occurring as part of the induced magnetosphere reconfiguration after the IMF rotation. The combined observations from MAVEN and Tianwen-1 provide a unique opportunity to study the Martian magnetosphere’s rapid response to changes in dynamic solar wind conditions. Future multipoint observations, incorporating MAVEN, Mars Express (MEX), Tianwen-1, and the upcoming ESCAPEDE mission (R. Lillis et al. 2024), will offer valuable insights into the origins and evolution of dynamic plasma processes such as magnetic reconnection and their roles in ion escape from the unique “hybrid” magnetosphere of Mars (G. A. DiBraccio et al. 2018).

Acknowledgments

We acknowledge NASA and the MAVEN mission for support through grant NNH10CC04C to the University of Colorado and by subcontract to Space Sciences Laboratory, University of California, Berkeley. We acknowledge Prof. Yuki Harada for helpful discussions at the MAVEN Reconnection Working Group Meeting. The research described in this Letter utilizes publicly available data from the MAVEN Science Data Center (<https://lasp.colorado.edu/maven/sdc/public/data/sci/>) and NASA Planetary Data System (<https://pds-ppi.igpp.ucla.edu/>), including data from the MAG (J. E. P. Connerney 2024), STATIC (J. P. McFadden 2024), SWIA (J. S. Halekas 2024), and SWEA (D. L. Mitchell 2024) instruments. We also acknowledge the Tianwen-1 MOMAG team for providing data access and support. The Tianwen-1/MOMAG data are publicly available at the Lunar and Planetary Data Release System (<https://moon.bao.ac.cn/web/enmanager/mars1>).

Appendix A Spacecraft Trajectories

Figure A1 illustrates the trajectories of the MAVEN and Tianwen-1 spacecraft during the observation period. Figure A1 also displays the magnetic field vector directions recorded by both spacecraft, providing an overview of the upstream IMF and the magnetic field configuration in the Martian magnetotail.

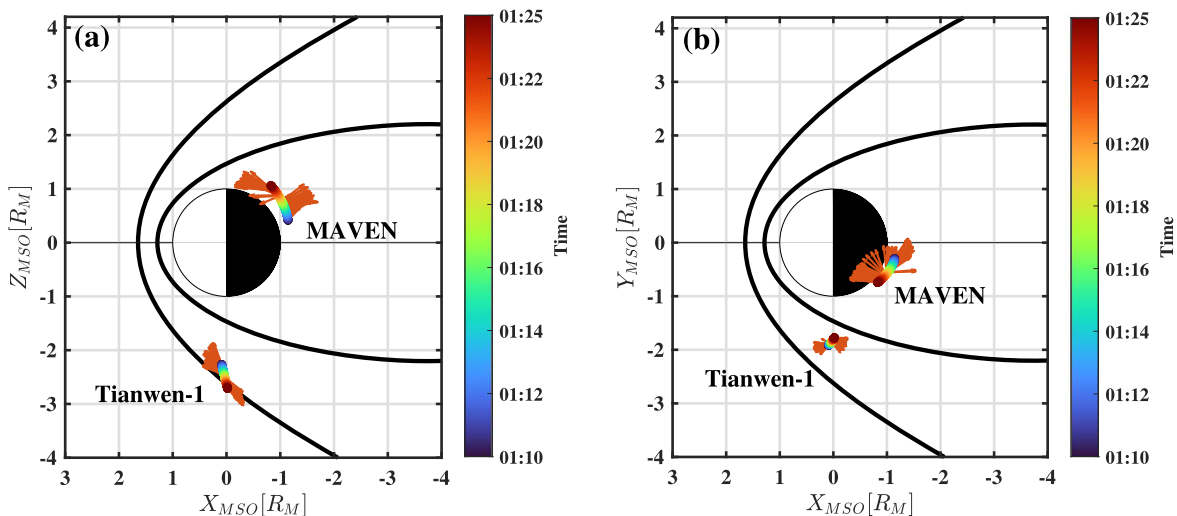


Figure A1. Tianwen-1 and MAVEN trajectories along with observed magnetic field vectors (orange arrows) in (a) the $X_{M_{SO}}-Z_{M_{SO}}$ plane and (b) the $X_{M_{SO}}-Y_{M_{SO}}$ plane.

Appendix B Walén Test Analysis

To further verify the occurrence of magnetic reconnection in the Martian magnetotail, we performed the Walén test using plasma and magnetic field measurements from MAVEN. The Walén test compares the observed plasma velocity changes across the current sheet with the predicted Alfvénic velocities

to assess whether the observed discontinuity is consistent with an Alfvénic outflow expected from reconnection. A strong correlation and slope close to unity between the observed and Alfvénic velocities indicate a reconnection event. The results of the Walén test are presented in Figure B1, which shows the comparison between the observed and Alfvénic velocity components.

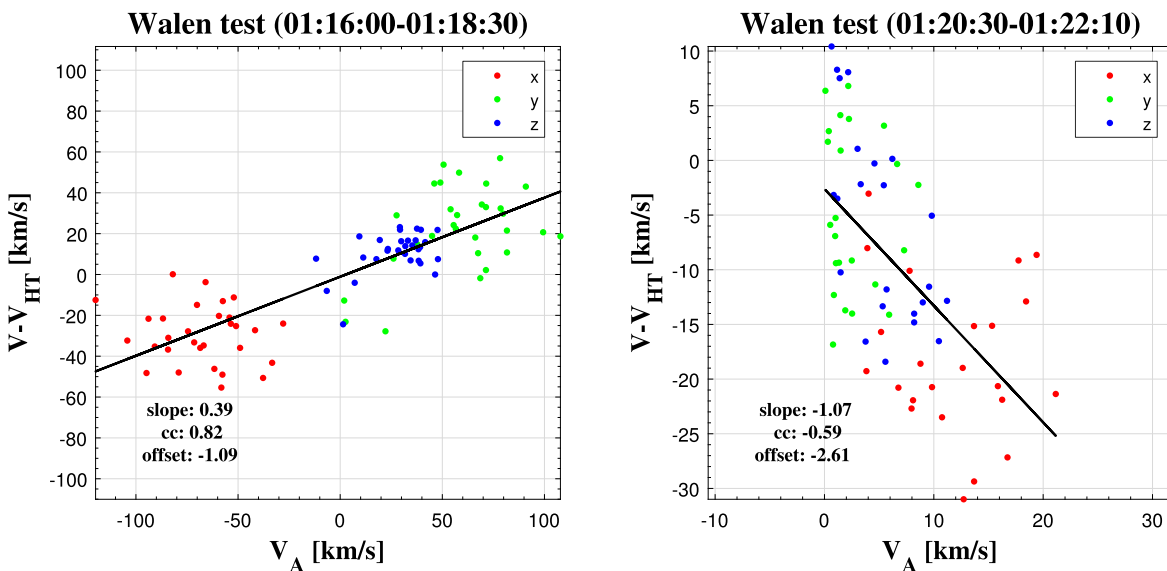


Figure B1. Scatter plot of averaged ion velocities in the Hoffmann–Teller (HT) frame vs. the Alfvén velocity before (left) and after (right) the current sheet crossing.

Appendix C Densities of Ions

Figure C1 illustrates the ion density variations during the observed reconnection event.

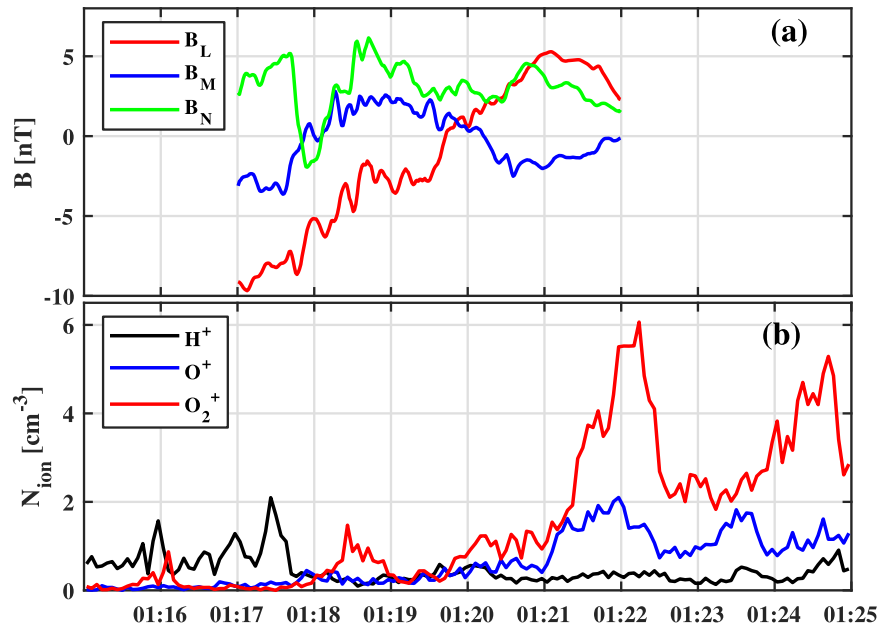


Figure C1. Panel (a) shows the magnetic field in LMN coordinates. Panel (b) shows densities of H^+ (black), O^+ (blue), and O_2^+ (red) in the time interval 01:15:00–01:25:00 UT.

ORCID iDs

Yuanzheng Wen <https://orcid.org/0000-0001-6141-6171>
 Jasper S. Halekas <https://orcid.org/0000-0001-5258-6128>
 Han-Wen Shen <https://orcid.org/0000-0001-6733-5065>
 Abigail R. Azari <https://orcid.org/0000-0002-8665-5459>
 David A. Brain <https://orcid.org/0000-0001-8932-368X>
 Yaxue Dong <https://orcid.org/0000-0003-3491-7506>
 David L. Mitchell <https://orcid.org/0000-0001-9154-7236>
 Christian X. Mazelle <https://orcid.org/0000-0001-5332-9561>
 Jared R. Espley <https://orcid.org/0000-0002-6371-9683>

References

- Acuna, M., Connerney, J., Ness, et al. 1999, *Sci*, 284, 790
 Azari, A., Abrahams, E., Sapienza, F., et al. 2023, *JGRA*, 128, e2023JA031546
 Bertucci, C., Achilleos, N., Dougherty, M., et al. 2008, *Sci*, 321, 1475
 Bertucci, C., Duru, F., Edberg, N., et al. 2011, *SSRv*, 162, 113
 Brain, D., Bagenal, F., Acuña, M., & Connerney, J. 2003, *JGRA*, 108, 1424
 Brain, D., Baker, A., Briggs, J., et al. 2010, *GeoRL*, 37, L14108
 Brain, D., Lillis, R., Mitchell, D., Halekas, J., & Lin, R. 2007, *JGRA*, 112, A09201
 Burch, J., Torbert, R., Phan, T., et al. 2016, *Sci*, 352, aaf2939
 Chen, G., Huang, C., Zhang, Y., et al. 2023, *ApJ*, 952, 37
 Connerney, J., Espley, J., Lawton, P., et al. 2015, *SSRv*, 195, 257
 Connerney, J. E. P. 2024, MAVEN MAG Tabulated vector magnetic field vs. time in payload coordinates Data Collection, NASA Planetary Data System, doi:10.17189/1414249
 Cravens, T., Fowler, C. M., Brain, D., et al. 2020, *JGRA*, 125, e2020JA028036
 De Hoffmann, F., & Teller, E. 1950, *PhRv*, 80, 692
 DiBraccio, G. A., Dann, J., Espley, J. R., et al. 2017, *JGRA*, 122, 4308
 DiBraccio, G. A., Luhmann, J. G., Curry, S. M., et al. 2018, *GeoRL*, 45, 4559
 DiBraccio, G. A., Romanelli, N., Bowers, C. F., et al. 2022, *GeoRL*, 49, e2022GL098007
 Dubinin, E., Fraenz, M., Pätzold, M., et al. 2023, *JGRA*, 128, e2022JA030575
 Dubinin, E., Modolo, R., Fraenz, M., et al. 2019, *GeoRL*, 46, 12722
 Eastwood, J., Brain, D., Halekas, J., et al. 2008, *GeoRL*, 35, L02106
 Ebert, R. W., Allegrini, F., Bagenal, F., et al. 2017, *GeoRL*, 44, 4401
 Edberg, N. J., Nilsson, H., Futaana, Y., et al. 2011, *JGRA*, 116, A09308
 Fan, K., Wei, Y., Fraenz, M., et al. 2023, *GeoRL*, 50, e2023GL103999
 Gao, J., Rong, Z., Klinger, L., et al. 2021, *E&SS*, 8, e2021EA001860
 Gershman, D. J., Fuselier, S. A., Cohen, I. J., et al. 2024, *SSRv*, 220, 7
 Gosling, J. 2012, *SSRv*, 172, 187
 Guo, Z., Fu, H., Cao, J., et al. 2024, *GeoRL*, 51, e2024GL112399
 Guo, Z., Liu, Y., Fu, H., et al. 2022, *ApJ*, 933, 128
 Halekas, J., Eastwood, J., Brain, D., et al. 2009, *JGRA*, 114, A11204
 Halekas, J., Taylor, E., Dalton, G., et al. 2015, *SSRv*, 195, 125
 Halekas, J., Ruhunusiri, S., Harada, Y., et al. 2017, *JGRA*, 122, 547
 Halekas, J. S. 2024, MAVEN SWIA Calibrated Coarse Survey 3D Data Collection, NASA Planetary Data System, doi:10.17189/1414231
 Halekas, J. S., Luhmann, J. G., Dubinin, E., & Ma, Y. 2021, *Magnetospheres in the Solar System* (New York: Wiley), 391
 Harada, Y., Halekas, J., DiBraccio, G., et al. 2018, *GeoRL*, 45, 4550
 Harada, Y., Halekas, J., McFadden, J., et al. 2015, *GeoRL*, 42, 8838
 Harada, Y., Halekas, J., McFadden, J., et al. 2017, *JGRA*, 122, 5114
 Hasegawa, H., Argall, M., Aunai, N., et al. 2024, *SSRv*, 220, 68
 Inui, S., Seki, K., Sakai, S., et al. 2019, *JGRA*, 124, 5482
 Jakosky, B. M., Lin, R. P., Grebowsky, J. M., et al. 2015, *SSRv*, 195, 3
 Joseph, J., Kurth, W. S., Sulaiman, A. H., et al. 2024, *JGRA*, 129, e2024JA033173
 Li, T., Liu, S., Yang, C., et al. 2023, *E&PP*, 7, 607
 Lillis, R., Curry, S., Curtis, D., et al. 2024, in *Lunar and Planetary Science Conf. 55* (Houston, TX: USRA), 1504
 Lin, R., Huang, S., Yuan, Z., et al. 2023, *ApJ*, 960, 68
 Lin, R., Huang, S., Yuan, Z., et al. 2024, *GeoRL*, 51, e2024GL108880
 Liu, K., Hao, X., Li, Y., et al. 2020, *E&PP*, 4, 384
 Liu, Y., Mouikis, C., Kistler, L., et al. 2015, *JGRA*, 120, 3535
 Ma, Y., Nagy, A. F., Hansen, K. C., et al. 2002, *JGRA*, 107, 1282
 Masters, A., Eastwood, J., Swisdak, M., et al. 2012, *GeoRL*, 39, L08103
 McFadden, J., Kortmann, O., Curtis, D., et al. 2015, *SSRv*, 195, 199
 McFadden, J. P. 2024, MAVEN STATIC Calibrated Energy Flux: 16 Energy X 64 Solid Angle X 8 Mass Bins Data Collection, NASA Planetary Data System, doi:10.17189/1517753

- Mitchell, D., Mazelle, C., Sauvaud, J.-A., et al. 2016, *SSRv*, **200**, 495
- Mitchell, D. L. 2024, MAVEN Solar Wind Electron Analyzer (SWEA) Survey Rate 3D Electron Distributions Data Collection, NASA Planetary Data System, doi:[10.17189/1414252](https://doi.org/10.17189/1414252)
- Modolo, R., Chanteur, G. M., & Dubinin, E. 2012, *GeoRL*, **39**, L01106
- Nagy, A., Winterhalter, D., Sauer, K., et al. 2004, *SSRv*, **18**, 33
- Niedner, M. B., Jr. 1984, *GMS*, **30**, 79
- Phan, T., Dunlop, M., Paschmann, G., et al. 2004, *AnGeo*, **22**, 2355
- Poh, G., Espley, J. R., Nykyri, K., et al. 2021, *JGRA*, **126**, e2021JA029224
- Romanelli, N., DiBraccio, G., Modolo, R., et al. 2019, *GeoRL*, **46**, 10977
- Romanelli, N., Modolo, R., Leblanc, F., et al. 2018, *JGRA*, **123**, 5315
- Russell, C., Saunders, M., Phillips, J., & Fedder, J. 1986, *JGRA*, **91**, 1417
- Sakai, S., Seki, K., Terada, N., et al. 2023, *JGRA*, **128**, e2022JA030510
- Sánchez-Cano, B., Lester, M., Andrews, D. J., et al. 2022, *ExA*, **54**, 641
- Shen, H.-W., Halekas, J. S., McFadden, J. P., Gruesbeck, J. R., & Schnepf, N. R. 2024, *ApJ*, **975**, 175
- Sonnerup, B. U. 1998, *ISSIR*, **1**, 185
- Vech, D., Stenberg, G., Nilsson, H., et al. 2016, *JGRA*, **121**, 3951
- Vignes, D., Mazelle, C., Rme, H., et al. 2000, *GeoRL*, **27**, 49
- Wan, W., Wang, C., Li, C., Wei, Y., & Liu, J. 2020, *E&PP*, **4**, 331
- Wang, G., Xiao, S., Wu, M., et al. 2024, *JGRA*, **129**, e2023JA031757
- Wang, J., Yu, J., Ren, A., et al. 2023, *ApJ*, **944**, 85
- Wang, J., Yu, J., Xu, X., et al. 2021, *GeoRL*, **48**, e2021GL095426
- Wang, L., Huang, C., Du, A., et al. 2023, *GeoRL*, **50**, e2023GL104996
- Wang, L., Huang, C., Ge, Y., et al. 2022, *JGRE*, **127**, e2022JE007181
- Wang, Y., Zhang, T., Wang, G., et al. 2023, *E&PP*, **7**, 216
- Weber, T., Brain, D., Mitchell, D., et al. 2017, *JGRA*, **122**, 9777
- Xu, S., Weber, T., Mitchell, D. L., et al. 2019, *JGRA*, **124**, 1823
- Xu, X., Wang, X., Zhou, Z., et al. 2023, *ApJ*, **955**, 41
- Ye, Y., Xu, X., Lee, L.-C., et al. 2024, *NatAs*, **8**, 838
- Zhang, C., Nilsson, H., Ebihara, Y., et al. 2023a, *NatCo*, **14**, 6866
- Zhang, C., Rong, Z., Klinger, L., et al. 2022, *JGRE*, **127**, e2022JE007334
- Zhang, C., Rong, Z., Nilsson, H., et al. 2021, *ApJL*, **922**, L33
- Zhang, C., Rong, Z., Zhang, L., et al. 2023b, *JGRA*, **128**, e2022JA031232
- Zhang, T., Lu, Q., Baumjohann, W., et al. 2012, *Sci*, **336**, 567
- Zhang, Y. 2016, *NatSR*, **6**, 27592
- Zhang, Y., Shen, C., Marchaudon, A., et al. 2016, *JGRA*, **121**, 4103
- Zhou, J., Liu, K., Jarvinen, R., et al. 2024, *ApJ*, **976**, 7
- Zou, Y., Zhu, Y., Bai, Y., et al. 2021, *AdSpR*, **67**, 812
- Zou, Z., Wang, Y., Zhang, T., et al. 2023, *ScChE*, **66**, 2396